STUDYING THE COSMIC X-RAY BACKGROUND WITH XMM-NEWTON.

A. De Luca[1,2] and S. Molendi[1]

[1]Istituto di Astrofisica Spaziale e Fisica Cosmica, Via Bassini 15, I-20133 Milano, Italy
[2]Università di Milano Bicocca, Dipartimento di Fisica, Piazza della Scienza 3, I-20126 Milano, Italy

Abstract

We present a work in progress aimed at measuring the spectrum of the Cosmic X-ray Background (CXB) with the EPIC detectors onboard XMM-Newton. Our study includes a detailed characterization of the EPIC non X-ray background, which is crucial in making a robust measurement of the spectrum of CXB. We present preliminary results, based on the analysis of a set of Commissioning and Performance Verification high galactic latitude observations.

Key words: X-rays: diffuse background

1. Introduction

The discovery of a diffuse background radiation in the X-ray sky dates back to the birth of X-ray astronomy: the first evidence was obtained by Giacconi et al. (1962) during the same rocket experiment which led to the discovery of Sco X-1, the first extra-solar X-ray source. Later observations have demonstrated that the bulk of Cosmic X-ray Background (CXB) above energies of ≈2 keV is of extragalactic origin, due to sources below the detection threshold. The first wide band measures of the CXB were made by HEAO−1 (1977): the CXB spectrum in the 2÷10 keV range was well described by a simple power law with photon index ≈ 1.4 (Marshall et al. 1980). More recently, several investigations (ASCA GIS/SIS: Miyaji et al. 1998, Gendreau et al. 1995; ROSAT PSPC: Georgantopulos et al. 1996; SAX LECS/MECS: Vecchi et al. 1999) have confirmed the spectral shape but have shown differences of order 30% in the normalization. Barcons et al. (2000) showed that cosmic variance cannot account for the differences among the previous measures of the CXB intensity; such an uncertainty seriously affects the modelling and the interpretation of the CXB (see e.g. Pompilio 2000). A new, reliable measure of the CXB is thus required to improve the overall understanding of its nature.
The XMM-EPIC instruments (Turner et al. 2001; Strüder et al. 2001) have appropriate characteristics to study extended sources with low surface brighteness, offering an unprecedented collecting area (≈ 2000 cm^2) and good spectral resolution (2% @ 6 keV) over a broad energy range (0.2÷12 keV) and a wide field of view (≈ 15 arcmin radius). However these cameras suffer a rather high instrumental background (Non X-ray Background, NXB). A correct characterization and subtraction of the NXB component is thus the crucial step in order to study the lowest surface brighteness source of the sky.
In this work we deal only with the EPIC *MOS* cameras; the *pn* camera, having different characteristics, will require a different approach.

2. Characterization of Non X-ray Background

The EPIC NXB can be divided into two parts: an electronic noise component, which is important only at the lower energies (below ≈0.3 keV), and a particle-induced component which dominates above 0.3 keV and is due to the interaction of particles in the orbital environment with the detectors and the structures that surround them. The particle-induced NXB is the sum of two different components:

1. a *flaring* component. Clouds of low-energy (≈ 100 keV) particles (believed to be protons) in the magnetosphere can be focused by the telescope mirrors, reaching the detectors. These unpredictable episodes cause an up to 100 times (or even more) increase of the quiescent background rate. Data collected during these intervals are almost unusable, especially for the study of extended sources, and must be rejected with Good Time Interval (GTI) filtering.
2. a *quiescent* component. It is mostly due to the interaction of high energy (E ≥ a few MeV) particles with the detectors and the surrounding structures. To characterize the quiescent NXB we have analyzed a set of observations performed with the filter wheel in closed position:
   – the temporal behaviour is stable within an observation time scale; we have hints for a secular decrease in the period covered by the dataset (orbits 20÷84);
   – the spectrum is characterized by a flat continuum, with several fluorescence emission lines from materials in the detectors or the surrounding structures (see Fig. 1);
   – the spatial distribution has a radially flat profile (within 10 %), but Al-K and Si-K line emission are highly anisotropic due to an illumination effect.

Proc. Symposium *'New Visions of the X-ray Universe in the XMM-Newton and Chandra Era'* 26–30 November 2001,

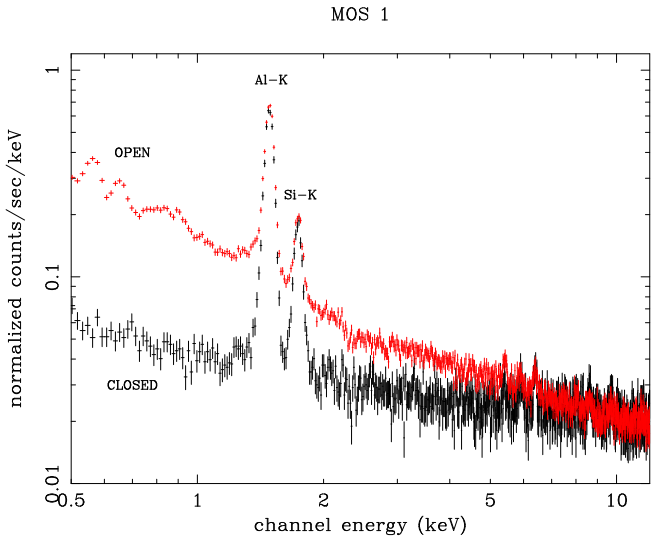

Figure 1. MOS1 quiescent NXB spectrum obtained from ≈100 ks of closed observations. For a comparison, the spectrum extracted from ≈ 200 ks of high galactic latitude observations of blank fields is also plotted (labelled OPEN). The closed spectrum is characterized by a flat continuum with bright fluorescence emission lines. The open spectrum is the sum of CXB and quiescent NXB.

Further closed observation are now being collected to improve the quiescent NXB characterization.

3. Subtraction of Non X-ray Background

A standard recipe to remove the NXB recovering the "pure" CXB spectrum could be sketched as follows:

1. standard processing and event reconstruction;
2. rejection of hot pixels and bad columns;
3. GTI filtering (removing the flaring NXB component);
4. extraction of the spectrum from a selected area;
5. subtraction of quiescent NXB spectrum.

This algorithm is indeed quite dangerous, since GTI filtering possibly leaves a low level Soft Proton (SP) NXB component unrejected; such a component could affect the CXB spectrum determination. In order to avoid this, we developed a simple diagnostic.
Since SP are focused by the mirrors, we have studied the correlation between counts extracted from the regions of the detectors which are inside (IN FOV) and outside (OUT FOV) the field of view of the telescopes. We applied to the OUT FOV event lists the same GTI computed for the corresponding IN FOV data. For each observation we extracted the counts (PATTERN $0 \div 4$) in the $8 \div 12$ keV band (where the CXB is negligible wrt. the NXB) from appropriate regions: in the IN FOV region we rejected CCD 1, where possibly CXB is not negligible, and we applied geometric masks to screen the brightest sources; in both the IN FOV and the OUT FOV regions we further applied geometric masks to reject the region spatially coincident with the underlying CCD 1 readout node (Au line emission).

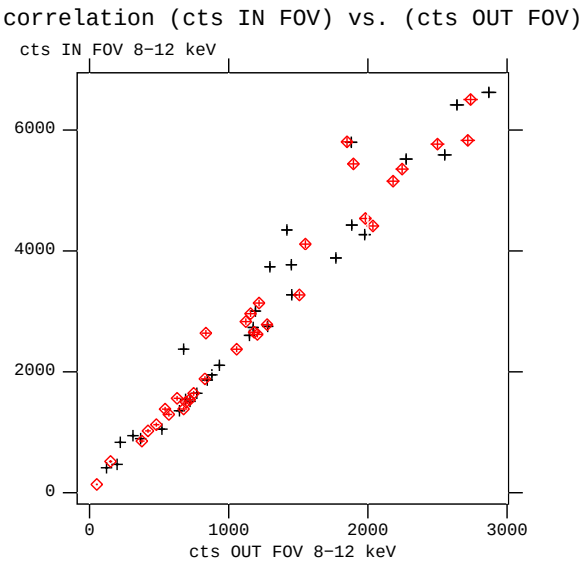

Figure 2. Plot of counts IN FOV vs. counts OUT FOV. Each point represents an observation: MOS1 black crosses, MOS2 red diamonds.

The main results are contained in Figures 2 and 3. Figure 2 shows that a good correlation exists between counts IN FOV and OUT FOV; however some scatter is present, possibly associated with anomalous counts IN FOV. Figure 3 shows that the ratio (counts IN FOV)/(counts OUT FOV) strongly correlates with the count rate IN FOV: the cluster of points in the lower left part of the graph represent the correct behaviour, while the correlation of the scattering points with the count rate IN FOV is a possible demonstration of the presence of some SP contamination.

These results can be used in two ways. First, we select the observations having a stable ratio (IN FOV)/(OUT FOV), within a maximum scatter of 15%, rejecting pathological cases. Second, if we suppose that the contaminating component has a spectral shape similar to the quiescent NXB (from closed observations), the value of the ratio (IN FOV)/(OUT FOV) can be used to try a renormalization of the quiescent background spectrum to be subtracted, in order to have

$$\left(\frac{IN}{OUT}\right)_{open} = \left(\frac{IN}{OUT}\right)_{closed}$$

4. Data acquisition, reduction and analysis

This work is based on a set of Commissioning, Performance Verification and GT observations selected among

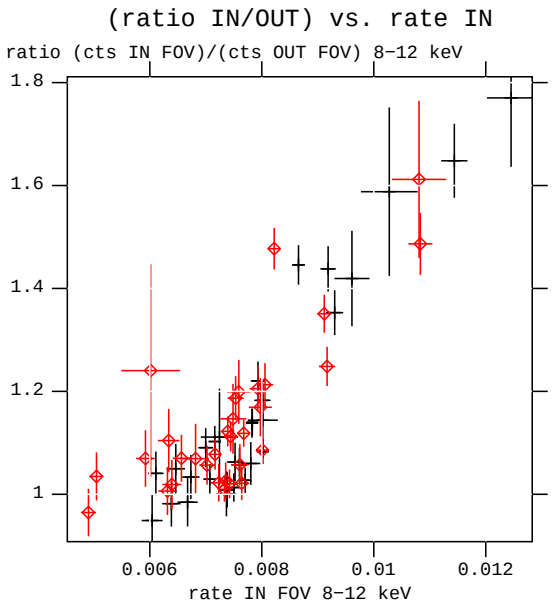

Figure 3. Plot of the ratio (cts IN FOV)/(cts OUT FOV) vs. count rate IN FOV. Each point represents an observation: MOS1 black crosses, MOS2 red diamonds.

high galactic latitude ($|\ b\ | > 27°$) pointings in order to avoid contamination by our galaxy; we discarded Magellanic Clouds pointings and observations of very bright sources. The closed observations collected during the very early orbits (≤ 40) were rejected, possibly being not fully reliable.

We used the XMM-Newton Science Analysis System (XMM -SAS) v.5.0 to perform the standard processing of the raw event lists. The linearized event lists were then cleaned from hot pixels and bad columns using an ad-hoc developed procedure which uses cosmic ray IRAF tasks to localize the pixels to be rejected in each CCD and XMM-SAS task *evselect* to remove them. Next step was GTI filtering to avoid flaring NXB intervals: we set a threshold of 0.29 cts/s in the energy range 8÷12 keV, rejecting also the time bins having 0 counts. The event files from closed observations were merged in a single list for each camera. For each observation a geometric mask was created and applied to reject an eventually present bright central source. The diagnostic described in 3 was then applied to verify the level of SP contamination. For each selected observation, we defined the best area to extract the CXB spectrum by a simple Signal to Noise ratio optimization (we remember that the signal of CXB is vignetted, while the instrumental NXB is not, so the S/N decreases with increasing off-axis angles). The spectrum were then extracted using an ad-hoc developed task which corrects for the telescope vignetting on an event-by-event logic, using the most recent vignetting function determinations and accounting for the azimuthal modulation induced by the RGA. The same routine is used to extract the NXB spectrum from the closed event list; the region of extraction is chosen in order to coincide in detector coordinates to the one used for the corresponding observation of the sky.

For each observation a tentative "pure" CXB spectrum is obtained with a simple subtraction of the NXB spectrum. A second spectrum is obtained after a renormalization of the NXB spectrum according to the prescription described in sect. 3.

5. Spectral analysis and results

The selected observations were 13 for MOS1 for a total good exposure time of 200 ks and 14 for MOS2 (210 ks). The CXB spectrum obtained for each observation was fitted using an absorbed power law model in the energy band 1.8-8 keV, setting N_H to 4×10^{20} cm^2; the normalization was computed at 4 keV. We computed the mean values of the CXB spectrum slope and intensity for each camera by a straight χ^2 minimization. Figure 4 shows the CXB spectrum extracted from an observation of the Lockman Hole field as seen by MOS1 (black) and MOS2 (red); exposure time is ≈ 30 ks per camera, the best fit power law model is superposed. The same analysis was performed

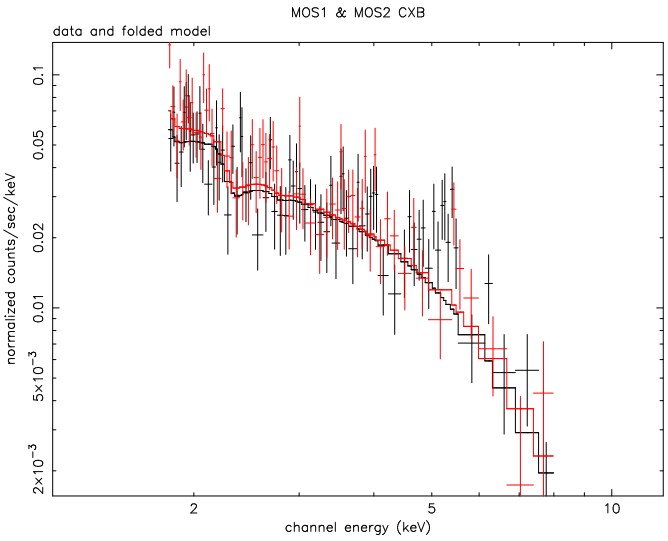

Figure 4. Spectrum of CXB for MOS1 (black) and MOS2 (red); Lockman Hole pointing; thick filter; ≈ 30 ks of exposure per camera. The best fit power law model is overplotted.

separately using the raw NXB spectrum and the renormalized one. The results are shown in Table 1. The *non-renormalized* case yields a correct value for the photon index, while the normalization is too high by $\approx 30\%$; on the contrary, the *renormalized* case yields a lower value for the normalization, but the photon index is too hard by $\approx 15\%$. The overall shape of the CXB spectrum has thus been correctly determined, being virtually coincident

Non renormalized case		
	Photon index	Intensity
MOS1	1.38±0.10	1.27±0.04
MOS2	1.44±0.09	1.29±0.05
Renormalized case		
	Photon index	Intensity
MOS1	1.52±0.11	1.01±0.04
MOS2	1.62±0.10	1.00±0.05

Table 1. Results of the spectral analysis. The parameters for the two cameras have been computed with a χ^2 minimization on the best fit values obtained for each observation. The intensity (@ 4 keV) is in units of 1.58 photons s^{-1} cm^{-2} keV^{-1} sr^{-1}, which corresponds (for a photon index equal to 1.4) to 11 photons s^{-1} cm^{-2} keV^{-1} sr^{-1} at 1 keV, an average value from previous measurements.

to previous determinations (see sect. 1); this means that the NXB spectrum has been properly characterized. The simple renormalization of NXB spectrum reduces by 30% the CXB intensity, but the results suggest that a more sophisticated procedure may be required.

6. Conclusions

Our study of the Cosmic X-ray Background is currently in progress. We obtained a characterization of the different NXB components for the MOS cameras. We showed that the standard GTI filtering to remove the flaring component possibly leaves a low-level SP NXB unrejected, and that the correlation of counts (IN FOV)/(OUT FOV) can provide a good diagnostic to identify and evaluate this effect, allowing to reject pathological cases. We tried to correct for SP contamination by means of a simple renormalization of the quiescent NXB spectrum. The preliminary results show that the CXB spectral shape is correct, but the intensity is too high by $\approx$ 30%. The renormalization approach is encouraging, but will require further study.

Acknowledgements

We would like to thank Dave Lumb for useful discussions. We are also grateful to all the members of the EPIC team for their work and for providing useful information and support.

References

Barcons, X., Mateos, S. and Ceballos, M. T., 2000, MNRAS 316, L13

Gendreau, K., Mushotzky, R., Fabian, A.C. et al., 1995, PASJ 47, L5

Georgantopulos, I., Stewart, G., Shanks, T. et al., 1996, MNRAS 280, 276

Giacconi, R., Gursky, H., Paolini, F. and Rossi, B., 1962, Phys. Rev. Lett. 9, 439

Marshall, F.E., Boldt, E.A., Holt, S.S. et al., 1980, ApJ 235, 4

Miyaji, T., Ishisaki, Y., Ogasaka, Y. et al., 1998, A&A 334, L13

Pompilio, F., La Franca, F. and Matt, G., 2000, A&A 353, 440

Strüder, L., Briel, U., Dennerl, K. et al., 2001, A&A,365, L18

Turner, M.J.L., Abbey, A., Arnaud, M. et al., 2001, A&A 365, L27

Vecchi, A., Molendi, S., Guainazzi, M., Fiore, F. and Parmar, A.N., 1999, A&A 349, L73